A Novel Boundary Preserving Adaptive Filter for Improving Superpixel's Compactness in Dental X-Ray Images

Maxwell A. Teixeira[1], **Domingos B. S. Santos**[1] **and Thelmo de Araujo**[1]

[1]Universidade Estadual do Ceará - UECE

{maxwell.alves, domingos.bruno}@aluno.uece.br, thelmo.araujo@uece.br

Abstract. *Superpixels techniques are commonly used on image segmentation because the objects's boundaries tend to be captured as a subset of the superpixels's boundaries. Superpixel's compactness is an important parameter for the quality of the final segmentation and it may be affected by image noise, which are very common in medical images. X-ray dental images are known to be particularly noisy. This paper analyzes the effects of smoothing and sharpening filters—frequently used in medical image preprocessing—on the compactness of the superpixels, measured by the isoperimetric quotient. Also, some experiments were conducted to validate two hypotheses about the causes of the filtering effects on the compactness of the superpixels. Based on the results, a boundary preserving adaptive filter (with several variants) is proposed, and its performance is compared to eight known filters: mean, median, Gaussian, gradient, Laplacian, morphological top hat, Kuwahara, and Kuwahara-Tomita filters. The proposed filter outperformed the filters tested here in increasing the overall compactness of the superpixels.*

Keywords: *Boundary preserving filters. Adaptive filters. Superpixel compactness. Dental X-ray image filters.*

1. Introduction

Superpixel algorithms oversegment an image into small patches that are perceptually meaningful and adhere well to the object boundaries [Chen et al. 2020]. These properties make superpixels very useful to medical image segmentation—among other applications, such as tracking and image search—, a difficult problem due to the noisy nature of the images. Segmentation of dental X-ray images is even a more challenging task for humans and machines and has many applications, such as caries detection, forensic identification, tooth segmentation, etc. [Silva et al. 2020].

The quality of a superpixel segmentation depends on many factors, such as stability, compactness, and run time. The compactness parameter is a measure of uniformity in shape and size of the superpixels and may be computed by several formulas [Neubert 2015].

It is common to preprocess the image before applying the segmentation algorithm in order to reduce noise or to sharpen object boundaries. Several filters may be used to this end and they may affect the resulting superpixels. In this paper, we show how applying common filters in X-ray dental images affect the compactness of the superpixels created by the SLIC algorithm.

The results of the application of the filters suggest two assumptions: The increase in smoothness (blur) of the image increases the compactness of the superpixels; The more compact are the superpixels, the better is the final segmentation. Experiments are conducted here in order to validate the assumptions. Based on the results, we propose an adaptive edge preserving filter that outperforms the analyzed filters regarding the compactness criterion.

This paper is organized as follows: Related papers are presented in Section 2. In Section 3, all known filters used in the experiments are explained. Section 4 presents the superpixels, the compactness measure, and the homogeneity measures used here. The proposed filters and the experiments are explained in Section 5. Finally, Section 6 presents the results and conclusions.

2. Related Work

Peer Neubert showed that segmentation stability and compactness are important properties of superpixel algorithms [Neubert 2015]. He also proposed a fast algorithm to create regularly shaped, compact superpixels by combining Seeded Watershed segmentation with compactness constraints. In the work of Stutz et al., the compactness of the superpixels was also emphasized, as the authors analysed 28 state-of-the-art superpixel algorithms [Stutz et al. 2018].

Schick et al. proposed a weighted mean of the isoperimetric quotient (see Equation 1) of the superpixels as a compactness measure and compared five superpixel algorithms: the normalized cuts segmentation, SLIC, TurboPixels, entropy rate superpixels, and Superpixel Lattices [Schick et al. 2012]. The authors showed that there is a trade-off between boundary recall and compactness and proposed an algorithm to control this trade-off.

In the seminal work of Kuwahara et al. [Kuwahara et al. 1976], an adaptive edge preserving filter was proposed to process RI-angiocardiographic images, removing noise while preserving the boundaries of the objets. Many variants of this filter have been proposed [Tomita and Tsuji 1977], [Nagao and Matsuyama 1979], etc.

Following different directions, many other edge preserving smoothing filters have still been proposed for different types of images (X-ray, MRI, CT), varying significantly in complexity and run time. Recent examples of these filters are presented in [Perumal and Manuel 2017] and [Rafati et al. 2018].

Filters based on mathematical morphology have been applied as preprocessing on medical images (blood vessel) with good segmentation results [Das et al. 2022].

To our knowledge, there is no published work comparing the effects of preprocessing filters on superpixel compactness.

3. Filters Overview

A digital filter maps each image pixel to some (linear or nonlinear) combination of pixels in an $n \times n$ neighborhood. Low-pass filters smooth the image in order to reduce noise, but tends to blur the objects's edges; high-pass filters sharpen objects's boundaries in the image at the cost of intensifying noise [Gonzalez and Woods 2017].

The most commonly used sharpening filters are based on first- and second-order derivatives: The gradient filter and the Laplace filter. Since Sobel gradient masks calculate derivatives in x and y directions, the magnitude of the filtered images is usually computed as the output. In order to sharpen the original image, a fraction of the result of the application of either gradient or Laplacian filters must be added to (or subtracted from) the original image.

For image smoothing, Gaussian filter and mean filter are universally used in preprocessing. The median filter is also frequently applied, being very effective to remove impulse noise. A Gaussian filter is usually applied to the original image before the application of sharpening filters.

Mathematical morphology may also be used to build noise reducing filters. Minkowski adition ($\oplus$) and subtraction ($\ominus$) define the basic morphological operators *dilation* ($\mathcal{D}$) and *erosion* ($\mathcal{E}$) [Shih 2009]:

$$\mathcal{D}(A, B) = A \oplus B = \cup_{b \in B}(A + b)\,,$$
$$\mathcal{E}(A, B) = A \ominus B = \cap_{b \in B}(A - b)\,,$$

where A is the image and B is the structure element.

Dilation and erosion may be combined into other morphological operators, like *opening* and *closing*, defined respectively by:

$$A \circ B = (A \ominus B) \oplus B = \mathcal{D}(\mathcal{E}(A, B))\,,$$
$$A \bullet B = (A \oplus B) \ominus B = \mathcal{E}(\mathcal{D}(A, B))\,.$$

Combinations of the opening and closing operators may be used to create filters like the *black top-hat* (which reduces small dark pixels) and the *white top-hat* (which reduces small bright pixels) filters [Das et al. 2022]:

$$\texttt{black\_tophat}(A, B) = (A \bullet B) - A\,,$$
$$\texttt{white\_tophat}(A, B) = A - (A \circ B)\,,$$

which, by their turn, may be combined into a filter commonly used in medical images and defined by:

$$\texttt{tophat}(A, B) = A + \texttt{black\_tophat}(A, B) - \texttt{white\_tophat}(A, B)\,.$$

Because smoothing tends to blur object's boundaries, some *boundary preserving* smoothing filters were proposed. The main idea is to analyze some pixel variability measure in a neighborhood of each pixel to determine the action to be executed.

One of the first boundary preserving filter was proposed by Kuwahara et al. in 1976: the variance of four $(k + 1) \times (k + 1)$ windows (shaded blocks in Figure 1) on the $(2k + 1) \times (2k + 1)$ neighborhood of each pixel (black blocks in Figure 1) is computed, and the mean filter is applied only to the pixels inside the $(k + 1) \times (k + 1)$ window with lowest variance [Kuwahara et al. 1976]. A Gaussian filter (or any other smoothing filter) may replace the mean filter.

In all the above filters, the size of the mask is the only parameter to be chosen by the user; in the Gaussian filter, the size may be determined by σ.

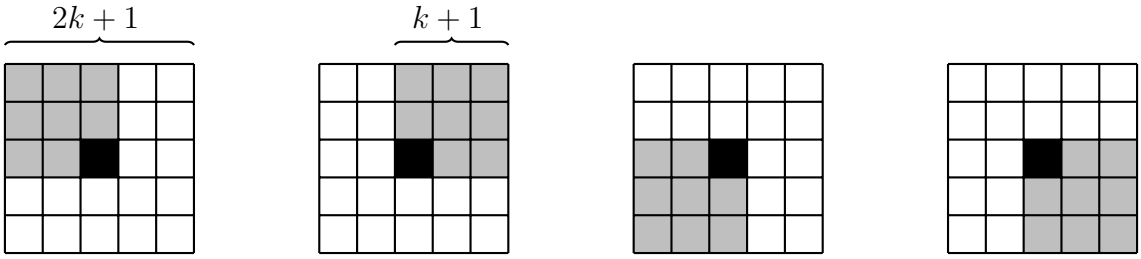

Figure 1. Kuwahara 5×5 masks.

4. Superpixels

The application of superpixel methods results in an oversegmented image, partitioned in such way that each partition element (called *superpixel*) tends to be perceptually uniform [Achanta et al. 2012]. The objects in the image may contain many superpixels, but ideally a superpixel should not be split by an object boundary, as seen in Figure 2. In order to obtain the desired segmentation, superpixels belonging to the same object must be grouped.

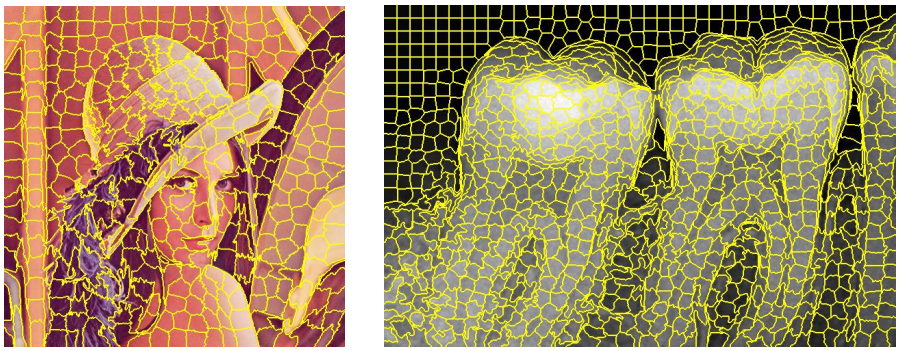

Figure 2. Examples of oversegmentated images using SLIC superpixel algorithm.

SLIC (Simple Linear Iterative Clustering) is the most commonly used superpixel algorithm, proposed by Achanta et al. in 2010. The SLIC algorithm uses a normalized sum of two distances: The first one is the 3D Euclidean distance in CIELAB color space, and the second one is the 2D Euclidean distance in the image plane. The clusters's centers are initialized and then perturbed, moving to the lowest color gradient in an $n \times n$ neighborhood [Achanta et al. 2012].

A desired property in superpixel algorithms is the compactness of the superpixels, as shown by Peer Neubert [Neubert 2015]. The compactness of an n-dimensional shape measures how close the shape is to the n-dimensional sphere. In the (bidimensional) plane, the most compact object is the circle.

4.1. Isoperimetric Quotient (IPQ)

A commonly used compactness measure is the *isoperimetric quotient*, defined by the rate between the area of the object, A, and the area of the circle, A_0, with the same perimeter [Schick et al. 2012]:

$$IPQ = \frac{A}{A_0}.$$

If p is the perimeter of the object, then the radius of the circle with the same perimeter is given by:

$$r = \frac{p}{2\pi}\,.$$

These equations give IPQ in terms of the area, A, and the perimeter, p, of the object:

$$IPQ = \frac{A}{\pi r^2} = \frac{A}{\pi\left(\frac{p}{2\pi}\right)^2} = \frac{A4\pi^2}{\pi p^2} = \frac{4\pi A}{p^2}\,. \tag{1}$$

The isoperimetric quotient is therefore a nondimensional number in the half-open interval $(0, 1]$. Being a compactness measure, the IPQ reaches its maximum in the circle, the most compact bidimensional object. In fact:

$$IPQ_{\text{circle}} = \frac{4\pi A}{p^2} = \frac{4\pi\left(\pi r^2\right)}{\left(2\pi r\right)^2} = 1\,.$$

Figure 3 shows some examples of bidimensional objects and their respective IPQ.

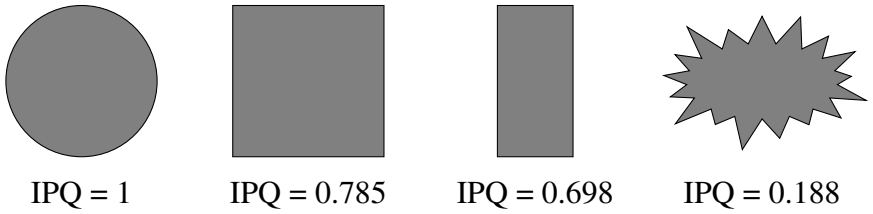

Figure 3. Examples of shapes with decreasing IPQ.

4.2. Region Homogeneity

A superpixel is designed to be perceptually homogeneous, and there are many ways to define the homogeneity of an image region. Some homogeneity measures for monochromatic images are defined below, but they may be extended to color images. Although all measures below are *reciprocally* related to the homogeneity of a region, except for GLCM homogeneity f_{hom}, they will still be called a homogeneity measure.

The simplest measure of homogeneity is the *variance* of the pixel intensity ($I(x, y)$) in the region of interest $\mathcal{R}$:

$$\sigma^2 = \frac{1}{N-1}\sum_{(x,y)\in\mathcal{R}}(I(x,y) - \overline{I})^2\,,$$

where N is the number of pixels in $\mathcal{R}$ and $\overline{I}$ is the average of the pixel intensities in $\mathcal{R}$.

The *contrast* may also be used as a homogeneity measure, and may be defined by:

$$C_M = \frac{\max(I(x,y)) - \min(I(x,y))}{\max(I(x,y)) + \min(I(x,y))}\,, \tag{2}$$

for $(x, y) \in \mathcal{R}$, as proposed in [Michelson 1927].

Based on the grey level co-occurrence matrix (GLCM) [Haralick et al. 1973], many homogeneity-like features may be calculated. The GLCM describes how often the pixels of an image make the transition from intensity i to intensity j, for a given angle θ (usually $0°, 45°, 90°$, and $135°$) and a given distance step d.

The following features are used in this paper, where $p(i, j)$ is the normalized (i, j)-element of the GLCM and G is the maximum gray level in the image:

$$f_{con} = \sum_{i=0}^{G}\sum_{j=0}^{G}(i-j)^2 p(i,j)\,, \qquad \text{(contrast)}$$

$$f_{diss} = \sum_{i=0}^{G}\sum_{j=0}^{G} p(i,j)\,|i-j|\,, \qquad \text{(dissimilarity)}$$

$$f_{hom} = \sum_{i=0}^{G}\sum_{j=0}^{G} \frac{p(i,j)}{1+(i-j)^2}\,, \qquad \text{(homogeneity)}$$

$$f_{ent} = -\sum_{i=0}^{G}\sum_{j=0}^{G} p(i,j)\,\log p(i,j)\,. \qquad \text{(entropy)}$$

5. Proposal and Experiments

In order to compare the results of filtering on the compactness of the superpixels, we selected only the most commonly used filters in the literature of medical image processing following two criteria: Low complexity, for a low run time; and the size of the window (σ for the Gaussian blur) should be the unique parameter to be chosen by the user.

5.1. Proposal

Experiments were conducted in order to check two assumptions: 1) The increase in smoothness (blur) of the image increases the compactness of the superpixels, because the blur tends to increase neighborhood's homogeneity. 2) The more compact are the superpixels, the better is the final segmentation, specially in medical images.

These assumptions, once validated, suggest the following modification of the Kuwahara filter: The algorithm initially checks the homogeneity of the $(2k+1)\times(2k+1)$ neighborhood centered in each pixel, if the homogeneity surpass a threshold value T, a smoothing filter is applied to the whole $(2k+1)\times(2k+1)$ neighborhood; otherwise, the Kuwahara filter is applied, that is, gray level variance is computed in the four $(k+1)\times(k+1)$ corner subwindows and the Gaussian blur is applied to the subwindow with the lowest value of variance. Algorithm 1 details the procedure.

One may notice that the Kuwahara filter only affects (blurs) a $(k+1)\times(k+1)$ neighborhood, although is applied to a $(2k+1)\times(2k+1)$ neighborhood of each pixel.

The proposed algorithm tends to smooth larger homogeneous regions than the classic Kuwahara filter, preserving objects's boundaries. All measures presented in Subsection 4.2 were tested as the homogeneity criterion for the proposed filter.

Algorithm 1 Proposed filter

Input: `image`, `kernel_size` $= 2k + 1$
Output: `blurred_image`

`feature_image` ← homogeneity_feature(`image`, $2k + 1$)
T ← threshold Otsu(`feature_image`)
`k-filtered_image` ← kuwahara(`image`, $2k + 1$)
`blurred_image` ← blur(`image`, $2k + 1$)
for each pixel i **do**
  if `feature_image`$(i) > T$ **then**
    `blurred_image`(i) ← `k-filtered_image`(i)
  end if
end for
return `blurred_image`

5.2. Databases

The dataset includes 120 digital periapical X-ray radiograph images [Rad et al. 2016, Rad et al. 2013, Rad et al. 2017, Rad et al. 2015]. The dimensions of the gray level images are 748×512 (width×height). The last 12 rows of each image contain some text information and were removed for our experiments, resulting in 748×500 images.

An auxiliary dataset was used to verify one of our working assumptions, which needs the segmentation ground truth masks. The dataset has 210 ultrasound images with 510×470 pixels each, which are another kind of noisy medical image, and their corresponding binary ground truth masks [Al-Dhabyani et al. 2020].

5.3. Experiments

All the experiments were implemented in Python language using NumPy, OpenCV, and scikit-image libraries. The `fast_glcm.py` library was used to compute the GLCM features [Izumi 2022].

In order to validate the assumption that the increase in smoothness increases the compactness of the superpixels, a simple experiment was implemented: The dataset images were smoothed by a mean filter with 10 different window sizes ($n \times n$, with $n = 3, 5, \ldots, 21$). Then, the SLIC algorithm was applied to the resulting image and the average compactness (IPQ) over all superpixels and images was calculated. Figure 4 (left) shows the results. Similarly, 10 different Gaussian filters, with $\sigma = 1.0, 1.5, \ldots, 5.5$, were applied to the images, followed by the SLIC algorithm, and the average compactness over all superpixels and images was calculated. Figure 4 (right) shows the results. As one may see in both plots in Figure 4, the larger the smoothing filter window size is, the more compact the superpixels become.

A dataset of medical images with ground truth masks [Al-Dhabyani et al. 2020] was necessary to validade our second assumption: Compact superpixels tend to improve final segmentation. Mean and Gaussian blur filters were used again to smooth the images before the SLIC algorithm is applied. Then, the resulting superpixels intersecting the ground truth mask were select and its the IoU (Intersection over Union) accuracy mea-

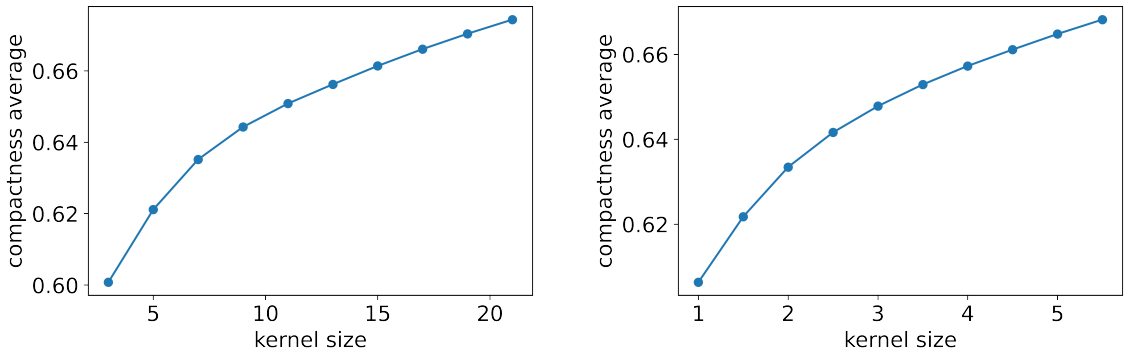

Figure 4. Effects of window size of mean (left) and Gaussian (right) filters on superpixel compactness average.

sure was calculated for each image. This procedure removes the dependence of the IoU measure on a classification algorithm. Figure 5 shows the reasonability of the assumption.

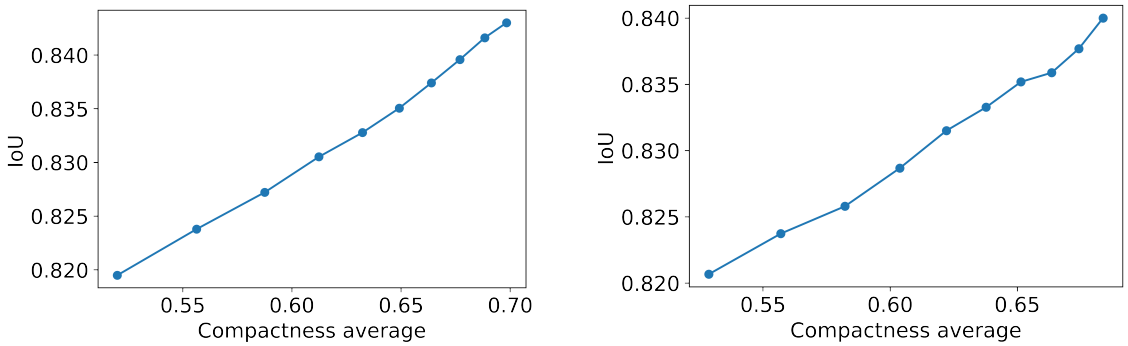

Figure 5. Effects of superpixel compactness on IoU: mean filter (left) and Gaussian blur (right).

The reasonability of both assumptions justified the creation of our boundary preserving adaptive filter based on Kuwahara's filter, as explained in Subsection 5.1. We then proceeded with the comparison of the performance of 8 known filters and 18 variants of the proposed filter.

The experiments consisted of applying the following filters to the dental X-ray images in the database, followed by the application of the SLIC algorithm to generate the superpixels. Then, the average of superpixels's compactness (IPQ) was computed for comparison.

26 filters were tested: mean, median, Gaussian, top-hat, gradient (Sobel), Laplacian, Kuwahara, Tomita and Tsuji, Proposal 1 (variance), Proposal 2 (contrast), Proposal 3 (GLCM contrast), Proposal 4 (GLCM dissimilarity), Proposal 5 (GLCM homogeneity), and Proposal 6 (GLCM entropy). All proposed filters were tested with 3 different types of blur: mean, median, and Gaussian blur. The GLCM features used $d = 1$ as the distance parameter and four angles: $0°, 45°, 90°$, and $135°$; the four resulting feature images were then averaged.

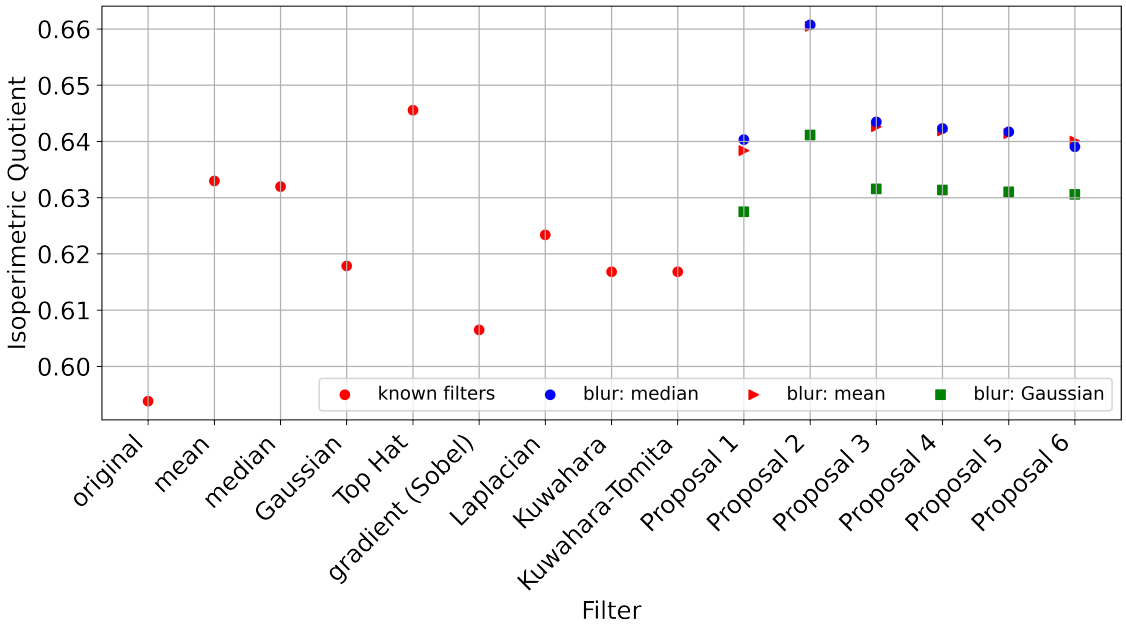

Figure 6. Effects of filters on superpixels's compactness.

6. Results ans Conclusions

Figure 6 shows the effects of the application of the 26 filters on the overall compactness of the superpixels generated by the SLIC algorithm applied to the set of 120 X-ray dental images. Applying the SLIC algorithm to the original images without any filter results on the lowest compactness average; this may be expected since noise affects the superpixels's boundaries, decreasing their compactness.

Among the known filters, the morphological top-hat filter achieved the best performance, and the Sobel gradient filter was the worst. The Kuwahara and the Kuwahara-Tomita filters had similar performances, both very close to the Gaussian blur.

The best overall result was achieved by the *proposed filter 2*, that uses *contrast* (Equation 2) as the homogeneity measure test and the *median blur* (using the mean blur achieved a very similar result). The other proposed filters obtained good results, outperforming the tested known filters, except for the top-hat filter.

Figure 7 shows an example of an original image and the result of applying the proposed filter using contrast as the homogeneity measure, median blur, and kernel size 11×11.

It is worth noticing that the median blur (using a $(2k+1) \times (2k+1)$ kernel) acted in only approximately 20% of the pixels, so 80% of the pixels were smoothed by a $(k+1) \times (k+1)$ kernel of the Kuwahara filter. All proposed filters presented similar percentages.

Another factor one should consider when using a filter is the run time, specially if the filter is applied to a large set of images. Figure 8 shows the run time of the experiments with all filters, including applying the SLIC algorithm and the computation of the IPQ. Considering the first point in Figure 8 as the baseline (since no filter was applied), one

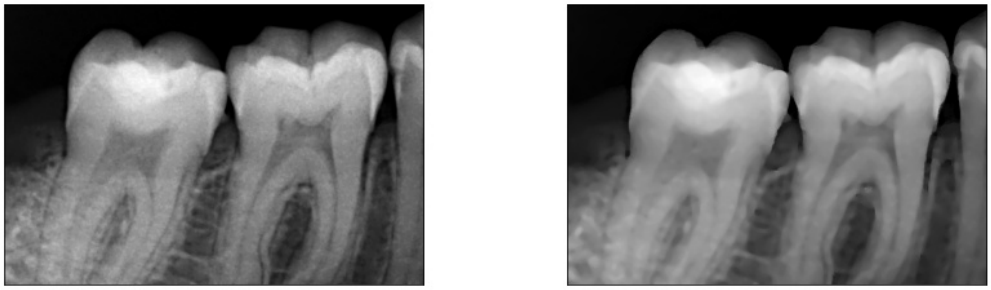

Figure 7. Original (left) and filtered image (right) example.

may notice that the filters had similar run times, except for the ones using GLCM features as the homogeneity test. This is easily understandable since a gray level co-occurancy matrix has to be calculated for each pixel in the image, which takes a toll on the run time. The *proposed filter 2* (*contrast* with *median blur*) run time is compatible with the run time of all the known filters tested here.

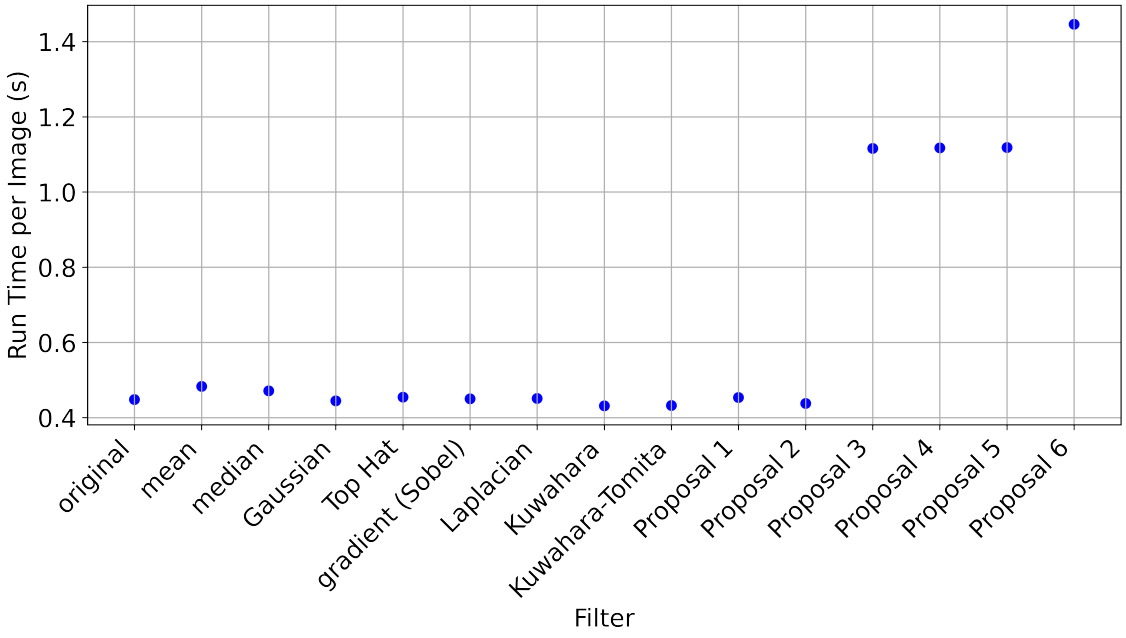

Figure 8. Run time of filters in the experiment.

In conclusion, the results show that the boundary preserving adaptive filter proposed, using contrast as the homogeneity measure and the median or mean blur, outperformed the most commonly used filters in the task of increasing the compactness of the superpixels applied to X-ray dental images. The filter is easy to implement and requires only a single parameter, viz. the kernel size. The proposed filter proved to be useful in preprocessing noisy medical images in order to increase segmentation accuracy.

Acknowledgments

This work was carried out with the support of Coordenação de Aperfeiçoamento de Pessoal de Nível Superior (CAPES).

References

Achanta, R., Shaji, A., Smith, K., Lucchi, A., Fua, P., and Süsstrunk, S. (2012). SLIC superpixels compared to state-of-the-art superpixel methods.

Al-Dhabyani, W., Gomaa, M., Khaled, H., and Fahmy, A. (2020). Dataset of breast ultrasound images. *Data in Brief*, 28(104863).

Chen, Z., Guo, B., Li, C., and Liu, H. (2020). Review on superpixel generation algorithms based on clustering. In *2020 IEEE 3rd International Conference on Information Systems and Computer Aided Education (ICISCAE)*, pages 532–537.

Das, T. P., Praharaj, S., Swain, S., Agarwal, S., and Kumar, K. (2022). Application of top-hat transformation for enhanced blood vessel extraction.

Gonzalez, R. C. and Woods, R. E. (2017). *Digital Image Processing*. Pearson Education, 4th edition.

Haralick, R. M., Shanmugam, K., and Dinstein, I. (1973). Textural features for image classification. *IEEE Transactions on Systems, Man, and Cybernetics*, SMC-3(6):610–621.

Izumi, T. (2022). Fast GLCM. `https://github.com/tzm030329/GLCM/blob/master/fast_glcm.py`.

Kuwahara, M., Hachimura, K., Eiho, S., and Kinoshita, M. (1976). *Processing of RI-Angiocardiographic Images*, pages 187–202. Springer US, Boston, MA.

Michelson, A. A. (1927). *Studies in Optics*. University of Chicago Press, Chicago, IL.

Nagao, M. and Matsuyama, T. (1979). Edge preserving smoothing. *Computer Graphics and Image Processing*, 9(4):394–407.

Neubert, P. (2015). *Superpixels and their Application for Visual Place Recognition in Changing Environments*. PhD thesis, Technische Universität Chemnitz, Sachsen, Germany.

Perumal, C. and Manuel, J. (2017). Sharpening of edges in radiographic images using edge preserving filter. *International Conference on Inventive Systems and Control (ICISC)*.

Rad, A. E., Amin, I., Rahim, M., and Kolivand, H. (2015). Computer-aided dental caries detection system from x-ray images. *Advances in Intelligent Systems and Computing*, 331:233–243.

Rad, A. E., Rahim, M., Rehman, A., Altameem, A., and Saba, T. (2013). Evaluation of current dental radiographs segmentation approaches in computer-aided applications. *IETE Technical Review*, 30:210–222.

Rad, A. E., Rahim, M., Shafry, M., Kolivand, H., and Amin, I. B. M. (2017). Morphological region-based initial contour algorithm for level set methods in image segmentation. *Multimedia Tools and Applications*, 76.

Rad, A. E., Rahim, M. S. M., Rehman, A., and Saba, T. (2016). Digital Dental X-ray Database for Caries Screening. *3D Research*, 7(2):18.

Rafati, M., Farnia, F., Taghvaei, M. E., and Nickfarjam, A. M. (2018). Fuzzy genetic-based noise removal filter for digital panoramic x-ray images. *Biocybernetics and Biomedical Engineering*, 38(4):941–965.

Schick, A., Fischer, M., and Stiefelhagen, R. (2012). Measuring and evaluating the compactness of superpixels. In *Proceedings of the 21st International Conference on Pattern Recognition (ICPR2012)*, pages 930–934.

Shih, F. H. (2009). *Image PProcessing and Mathematical Morphology: Fundamentals and Applications*. Taylor and Francis, Boca Raton, FL.

Silva, B., Pinheiro, L., Oliveira, L., and Pithon, M. (2020). A study on tooth segmentation and numbering using end-to-end deep neural networks. *2020 33rd SIBGRAPI Conference on Graphics, Patterns and Images (SIBGRAPI)*.

Stutz, D., Hermans, A., and Leibe, B. (2018). Superpixels: An evaluation of the state-of-the-art. *Computer Vision and Image Understanding*, 166:1–27.

Tomita, F. and Tsuji, S. (1977). Extraction of multiple regions by smoothing in selected neighborhoods. *IEEE Transactions on Systems, Man, and Cybernetics*, 7(2):107–109.